recovered reactant or in the product at the α carbon, because C_α–C_β bond rotation in the intermediate observed in the simulations would likely induce isomerization.

Analogous direct-MD simulations for Me_3CCH_2-OH_2^+ gave only concerted trajectories. In this case, the hypothetical cationic intermediate is an extremely unstable primary carbocation. Similarly, only concerted trajectories were observed for $MeOCMe_2CHMeOH_2^+$, in which MeO rather than Me is the migrating group. This difference is reasonable in light of the MeO group having a much larger migratory aptitude than Me, and hence $MeOCMe_2CHCH_3$-OH_2^+ having a much stronger preference for the concerted migration than $Me_3CCHMeOH_2^+$ (*15*). The different outcome for the different systems indicates that the observed dynamics-driven reaction paths for pinacolyl-OH_2^+ are a manifestation of the inherent nature of the reaction system.

These direct ab initio MD simulations for the intramolecular rearrangement reaction of protonated pinacolyl alcohol revealed that the reaction pathway did not follow the IRC pathway on the PES, but rather that it was controlled by the dynamics of the reaction. In most cases, the reaction is first initiated by the C-O bond cleavage to give a secondary carbocation intermediate, which may have a lifetime of up to 4000 fs. Then the intermediate cation yielded rearranged products, for an overall stepwise mechanism. This example shows that the reaction mechanism reflects the effects of reaction dynamics rather than simply the shape of the PES. It is very likely that similar findings will arise for many other reactions and that the characterization and interpretation of reaction mechanisms ought to consider the effects of dynamics explicitly. The reaction dynamics prefers the stepwise rather than the concerted pathway because the initial motion of the reacting species is toward the cationic region as a result of the shape of the energy surface. These results imply that a TS of a given character may have only limited importance with respect to the actual mechanism.

References and Notes

1. L. P. Hammett, *Physical Organic Chemistry: Reaction Rates, Equilibria, and Mechanisms* (McGraw-Hill, New York, ed. 2, 1970).
2. E. S. Lewis, Ed., *Investigation of Rates and Mechanisms of Reactions* (Wiley Interscience, ed. 3, New York, 1974).
3. B. K. Carpenter, *Acc. Chem. Res.* **25**, 520 (1992).
4. _____, *J. Am. Chem. Soc.* **117**, 6336 (1995).
5. K. Bolton, W. L. Hase, C. Doubleday Jr., *J. Phys. Chem. B* **103**, 3691 (1999).
6. L. Sun, K. Song, W. L. Hase, *Science* **296**, 875 (2002).
7. H. Yamataka, M. Aida, M. Dupuis, *Chem. Phys. Lett.* **353**, 310 (2002).
8. H. Yamataka, M. Aida, *Bull. Chem. Soc. Jpn.* **75**, 2555 (2002).
9. T. Ando, H. Morisaki, *Tetrahedron Lett.* **20**, 121 (1979).
10. F. P. Wilgis, T. E. Neumann, V. J. Shiner Jr., *J. Am. Chem. Soc.* **112**, 4435 (1990).
11. The ab initio calculations were performed with the Gaussian program package [M. J. Frisch *et al.*, Gaussian98 (Gaussian, Pittsburgh, PA, 1998)].
12. Details of the MD simulations and details of selected trajectories are available at *Science* Online.
13. P. J. Robinson, K. A. Holbrook, *Unimolecular Reaction* (Wiley, New York, 1972).
14. W. L. Hase, *Acc. Chem. Res.* **16**, 258 (1983).
15. J. March, *Advanced Organic Chemistry* (Wiley Interscience, New York, ed. 4, 1992).
16. The calculations were carried out in part at the Research Center for Computational Science, Okazaki National Research Institute. Supported in part by a Grant-in-Aid for Scientific Research from the Ministry of Education, Culture, Sports, Science, and Technology of Japan, and by a grant from Asahi Glass Foundation. S.C.A. thanks the Japan Society for the Promotion of Science for a fellowship. M.D. was supported by the U.S. Department of Energy's Office of Biological and Environmental Research, and the Office of Basic Energy Sciences, Chemical Physics Program. The Pacific Northwest National Laboratory is a multiprogram national laboratory operated for the U.S. Department of Energy by Battelle Memorial Institute under contract DE-AC06-76RLO 1830.

Supporting Online Material
www.sciencemag.org/cgi/content/full/299/5612/1555/DC1
Materials and Methods
Figs. S1 to S4
References

17 October 2002; accepted 21 January 2003

A Supershear Transition Mechanism for Cracks

Eric M. Dunham,[1]* Pascal Favreau,[2] J. M. Carlson[1]

Seismic data indicate that fault ruptures follow complicated paths with variable velocity because of inhomogeneities in initial stress or fracture energy. We report a phenomenon unique to three-dimensional cracks: Locally stronger fault sections, rather than slowing ruptures, drive them forward at velocities exceeding the shear wave speed. This supershear mechanism differentiates barrier and asperity models of fault heterogeneity, which previously have been regarded as indistinguishable. High strength barriers concentrate energy, producing potentially destructive pulses of strong ground motion.

Earthquakes are modeled as shear cracks propagating along fault planes. Heterogeneous stress and strength distributions lead to complex rupture histories. Because elastic waves radiate from the concentrated region of maximum sliding velocity at the rupture front, perturbations to its motion, particularly those inducing propagation faster than the shear wave speed, are the source of high-frequency ground motions (*1*). Material heterogeneity is characterized by regions of increased fracture energy, i.e., cohesive resistance to sliding, known as barriers (*2*). Alternatively, ruptures in the asperity model follow regions of high initial stress close to failure (*3*). This prestress variability is set by the residual stress field remaining from past events, combined with tectonic loading.

Spontaneous rupture occurs when the energy release rate (the flux of kinetic and strain energy from the prestress field into the rupture front) overcomes the local fracture energy. The trade-off between the energy that is supplied from the prestress field and the fracture energy results in an underdetermined problem, making it difficult to establish the source of fault heterogeneities (*4*, *5*). In fact, radiation from dynamic two-dimensional (2D) cracks is identical in barrier and asperity models (*1*). Recent advances in parallel computing enable us to investigate complex 3D dynamic rupture propagation.

Large strike-slip earthquakes occur predominantly in mode II (in which the slip is parallel to the direction of rupture propagation), for which the limiting velocity is usually the Rayleigh surface wave speed v_R. However, for a homogeneous medium with high prestress or low fracture energy, speeds between the shear wave speed v_S and longitudinal wave speed v_P are allowed (*6*–*10*). Intersonic propagation, although theoretically predicted (*7*), was only recently observed (*11*). Stable velocities are centered around $\sqrt{2}v_S$, a peculiar speed at which crack growth is similar to subsonic propagation (for example, the Mach cones extending from the rupture front vanish) (*9*, *10*, *12*, *13*).

Seismic data indicate that most earthquakes occur slightly below v_R. With the advent of strong motion seismograph networks in the near field, inversions and modeling of several major earthquakes suggest that supershear bursts occur on sections of the fault close to failure. These include the 1979 Imperial Valley (*14*), 1992 Landers (*15*), and 1999 Izmit, Turkey (*16*, *17*) earthquakes.

We modeled bilaterally expanding ruptures (shear cracks) by solving the elastodynamic wave equation in a 3D medium surrounding a

[1]Department of Physics, University of California, Santa Barbara, CA 93106, USA. [2]Institut de Physique du Globe de Paris, 75252 Paris, France.

*To whom correspondence should be addressed. E-mail: edunham@physics.ucsb.edu

rectangular planar fault. Slip, the relative shear displacement between the two sides of the fault, was constrained to be horizontal. We nucleated ruptures by initially overstressing a vertical section of the fault. We placed periodic boundary conditions in the vertical direction to simulate an infinite-width mode II crack and we placed absorbing boundary conditions to prevent reflections from all other sides. Perturbations to the rupture front introduced a component of mode III failure (i.e., a slip parallel to the rupture front).

A uniform compressive stress acted on the fault, which was governed by a fracture criterion relating shear traction to slip. In particular, we used a slip-weakening cohesive zone model that constrains material failure processes to the fault plane (*8*, *18*). The fault started at a prestress value, σ_0. Slip initiated when the shear stress reached a critical static friction stress level, σ_s, normalized to unity. The stress then decreased linearly with increasing slip over a characteristic distance (i.e., the slip-weakening distance d_c), after which the surfaces were left at a constant sliding friction value, σ_f, that we scaled to zero. For the unit area of the new fracture, the work done against cohesion was the fracture energy, $G = \sigma_s d_c/2$.

The supershear transition for 2D mode II cracks on homogeneous faults occurs only if the prestress is sufficiently high. A stress peak traveling at v_S ahead of a sub-Rayleigh rupture exceeds the static stress, allowing the crack to jump to intersonic velocities (*7*, *8*). Cracks become supershear after a distance (proportional to d_c) that diverges as the prestress approaches a numerically obtained critical value: $\sigma_0 = 0.38$ (*8*). For lower prestress values, the crack's terminal velocity is v_R. This mechanism does not apply to 3D cracks. Instead, the dimensionless ratio κ of the energy release rate ($\sim\sigma_0^2\lambda/\mu$, where μ is the shear modulus) to the fracture energy controls the supershear transition (*19*, *20*). The length scale λ determines the stress concentration at the rupture front (i.e., the stress intensity factor) and is specific to the geometry of the problem (for example, the fault width for a rectangular planar fault).

We investigated cracks with prestress $0.3 \leq \sigma_0 \leq 0.4$, which remained sub-Rayleigh in the absence of any perturbations over the length of our fault. We introduced a circular obstacle to the fault, either a barrier, which requires more energy to break, or an anti-asperity, which is a region of lower prestress that decreases the energy release rate. Either obstacle locally reduced κ, suggesting that the energy balance would favor slower propagation or even arrest of the rupture. Model parameters, including the obstacle size, were consistent with observations (*21*).

The anti-asperity model only slightly delays the rupture front, which moves to regain its unperturbed shape after breaking the obstacle (Fig. 1 and movie S1). The barrier model is much more complex (Fig. 1 and movie S2). The stress concentration at the rupture front is initially insufficient to break the barrier. The rupture temporarily halts as the stress grows to the higher static level inside. Meanwhile, the faster-moving rupture front outside of the barrier encircles it, breaking it from all sides. This is similar to the rupture of a single asperity of high prestress, initiated from a point on the edge of the asperity (*22*). The rupture fronts within the barrier converge almost to a point, resulting in a concentrated region of high slip velocity at the far side of the barrier. When the barrier breaks, it emits an elliptical slip velocity pulse moving at v_R in the direction parallel to slip and at v_S in the perpendicular direction, as well as a weaker pulse moving at v_P in the forward direction. Furthermore, the energy concentration induces the transition to a rupture velocity slightly less than $\sqrt{2}v_S$ (Fig. 2)

To explore this phenomenon, we varied both initial stress and barrier strength. We found that maximum slip velocities within the barrier scale linearly with static stress, rather than with the prestress that has been found in homogeneous models and has been assumed for all ground motion predictions (*23*, *24*). We refer to this effect, resulting in slip velocities over an order of magnitude larger than at the unperturbed front, as barrier focusing.

Barriers slightly stronger than the surrounding fault ($1 < \sigma_s < 1.3$) only mildly perturb the rupture front, which returns toward the stable planar configuration at a sub-Rayleigh speed (Fig. 3). Above a critical strength ($\sigma_s^* \approx 1.3$), the restoring motion

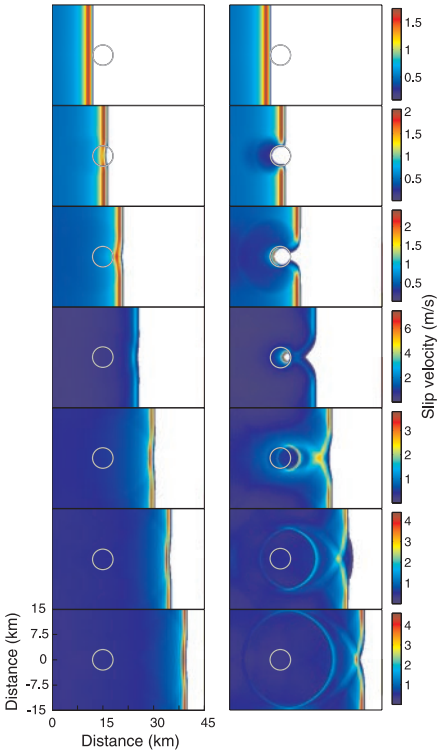

Fig. 1. Consecutive illustrations showing slip velocity on the fault plane for the anti-asperity (**left**) and barrier (**right**) models, both having κ locally decreased by a factor of 5. Locked regions of the fault are uncolored, and the gray circle marks the obstacle's perimeter. The color scale changes at each time step.

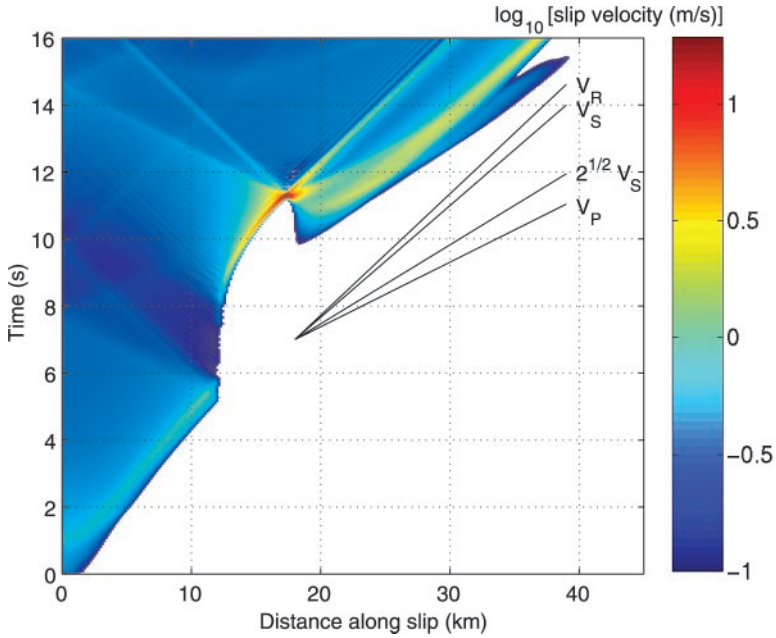

Fig. 2. Space-time plot of slip velocity along the symmetry axis through the center of the barrier, which lies at $x = 15$ km. The four black lines show wave speeds. Locked regions of the fault are uncolored.

becomes supershear with a duration that, like the slip velocity, increases linearly with barrier strength until $\sigma_s \approx 3.5$.

At the opposite extreme, when the barrier is much stronger than the surrounding fault ($\sigma_s \geq 7$), the rupture front splits as it breaks the material above and below the obstacle and coalesces on the far side into a region of high slip velocity. This is caused by rupture front focusing, in which two colliding fronts cause a rapid stress drop (*25*). The split-front focusing effect causes a burst of supershear propagation, with a duration independent of the barrier strength.

When the barrier breaks, it releases a slip velocity pulse traveling at v_P. If the rupture has not moved too far past the barrier, this pulse carries sufficient energy to enhance the duration of supershear propagation, which has already been activated by split-front focusing. Precise timing, occuring for $3.5 < \sigma_s < 7$, results in a resonance during which the supershear front moves ahead of the unperturbed front.

Further numerical experiments showed that weak anti-asperities ($\sigma_0 \leq 0$) induce a supershear transition as a result of split-front focusing. Low prestress values are necessary because the energy release rate into the rupture front is a nonlocal function of the prestress history (*26*). The size of the anti-asperity relative to the crack length precludes large variations of the energy release rate, making anti-asperities dynamically much less of an obstacle than barriers. An anti-asperity that takes the same amount of time to break as a $\sigma_s = 5$ barrier will have $\sigma_0 = -1.2$ and will produce only 0.65 times the spatial duration of supershear propagation. Furthermore, formation of a high-slip-velocity region within the anti-asperity does not occur as it does within the barrier (for which maximum slip velocity scales with the barrier strength). The anti-asperity with $\sigma_0 = -1.2$ produces only 13% of the maximum slip velocity observed within the barrier. This limits the amplitude of seismic waves released from the anti-asperity, and thus prevents the rupture front from overtaking its unperturbed position.

Our results show that existing parameters governing the supershear transition on a homogeneous fault cannot characterize the complex dynamics of heterogeneous faults. Despite such idealizations as a perfectly circular barrier with uniform properties, our simulations reveal unexpected phenomena that may be common at many scales. Because ground motion is proportional to slip velocity (*24*), barrier focusing releases intense seismic waves. Near-field seismograms from the 1984 Morgan Hill earthquake show, in addition to the usual phases from the hypocenter, a second large pulse in ground motion arriving about 8 s later that can be traced to a region 14 km along the strike from the hypocenter (*27*, *28*). Kinematic inversions suggest that the region failed after being encircled by the rupture front (*28*), making this a likely candidate for our mechanism. The extreme amplitudes of these pulses make them potentially destructive, suggesting that the identification of currently unbroken barriers (from inversions of past events) must become a part of seismic hazard analysis.

On a smaller scale, our results apply to dynamic shear fracture of brittle engineering materials. Laboratory experiments provide a convenient framework for analysis of our phenomena. Furthermore, barrier focusing, and the corresponding scaling of slip velocity with static stress rather than prestress, is unique to 3D cracks. This scaling, which implies a local independence from external loading, runs counter to fundamental fracture mechanics assumptions and likely extends to dynamic tensile failure of brittle materials that are common in engineering applications.

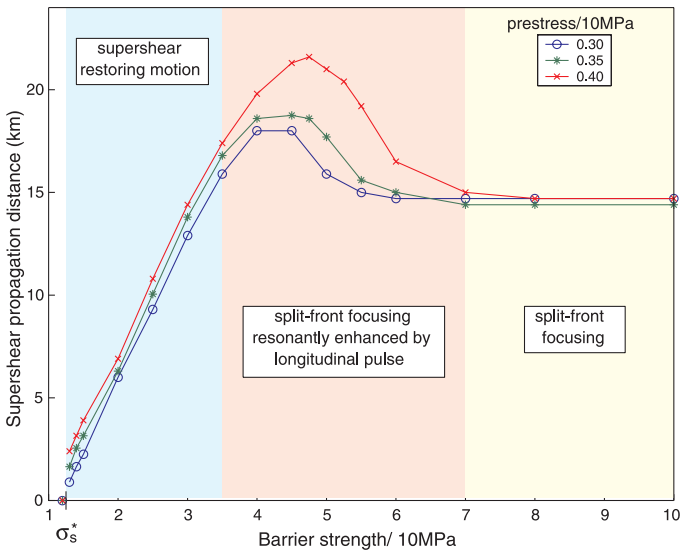

Fig. 3. Dependence of supershear propagation on barrier strength and prestress. The background colors indicate the mechanism governing the supershear transition.

References and Notes

1. R. Madariaga, *Ann. Geophys.* **1**, 17 (1983).
2. S. Das, K. Aki, *J. Geophys. Res.* **82**, 5658 (1977).
3. H. Kanamori, G. Stewart, *J. Geophys. Res.* **83**, 3427 (1978).
4. M. Guatteri, P. Spudich, *Bull. Seismol. Soc. Am.* **90**, 98 (2000).
5. S. Peyrat, K. B. Olsen, R. Madariaga, *J. Geophys. Res.* **106**, 26467 (2001).
6. The energy release rate is a monotonically decreasing function of rupture velocity that vanishes at v_R. Steady-state propagation between v_R and v_S is forbidden as the energy flux into the rupture front becomes negative (*9*, *10*, *12*). Generalization to a process region of finite length at the rupture front allows for a nonzero energy release rate at intersonic velocities.
7. R. Burridge, *Geophys. J. R. Astron. Soc.* **35**, 439 (1973).
8. D. J. Andrews, *J. Geophys. Res.* **81**, 5679 (1976).
9. K. B. Broberg, *Geophys. J. Int.* **119**, 706 (1994).
10. _____, *Arch. Mech.* **47**, 859 (1995).
11. A. J. Rosakis, O. Samudrala, D. Coker, *Science* **284**, 1337 (1999).
12. R. Burridge, G. Conn, L. B. Freund, *J. Geophys. Res.* **85(B5)**, 2210 (1979).
13. L. B. Freund, *J. Geophys. Res.* **84(B5)**, 2199 (1979).
14. R. J. Archuleta, *J. Geophys. Res.* **89**, 4559 (1984).
15. K. B. Olsen, R. Madariaga, R. J. Archuleta, *Science* **278**, 834 (1997).
16. M. Bouchon *et al.*, *Geophys. Res. Lett.* **27**, 3013 (2000).
17. M. Bouchon *et al.*, *Geophys. Res. Lett.* **28**, 2723 (2001).
18. Y. Ida, *J. Geophys. Res.* **77**, 3796 (1972).
19. R. Madariaga, S. Peyrat, K. B. Olsen, in *Problems in Geophysics for the New Millennium*, E. Boschi, G. Ekström, A. Morelli, Eds. (Editrice Compositori, Bologna, Italy, 2000), pp. 89–110.
20. R. Madariaga, K. B. Olsen, *Pure Appl. Geophys.* **157**, 1981 (2000).
21. We measure distances in terms of the uniform grid spacing, and scale $\mu = 1$ and $v_S = 1$. We set the obstacle diameter to $D = 40$ and slip-weakening distance to $d_c = 10$. Rescaling to physical units is accomplished by multiplying distances (in grid points) by $(\mu/30\ \text{GPa})[10\ \text{MPa}/(\sigma_s - \sigma_f)](d_c/50\ \text{cm})150$ m, by multiplying time (in steps) by $(\mu/30\ \text{GPa})[10\ \text{MPa}/(\sigma_s - \sigma_f)](d_c/50\ \text{cm})[(3\ \text{km/s})/v_S]0.05$ s, and by multiplying slip velocities by $(30\ \text{GPa}/\mu)[(\sigma_s - \sigma_f)/10\ \text{MPa}][v_S/(3\ \text{km/s})]$m/s, as has been done for the figures. Thus the barriers are 6 km in diameter.
22. S. Das, B. Kostrov, *J. Geophys. Res.* **88**, 4277 (1983).
23. J. Brune, *J. Geophys. Res.* **75**, 4997 (1970).
24. K. Aki, P. Richards, *Quantitative Seismology* (University Science Books, Sausalito, CA, 2002).
25. E. Fukuyama, R. Madariaga, *Pure Appl. Geophys.* **157**, 1959 (2000).
26. L. B. Freund, *Dynamic Fracture Mechanics* (Cambridge Univ. Press, Cambridge, 1989).
27. S. Hatzell, T. Heaton, *Bull. Seism. Soc. Am.* **76**, 649 (1986).
28. G. Beroza, P. Spudich, *J. Geophys. Res.* **93**, 6275 (1988).

29. E.D. acknowledges the support of an Office of Naval Research–National Defense Science and Engineering Graduate fellowship. This work was supported by the David and Lucile Packard Foundation, NSF (grant DMR-9813752); and a grant from the Keck Foundation, which established an Interdisciplinary Program in Seismology and Materials Science at the University of California, Santa Barbara.

Supporting Online Material

www.sciencemag.org/cgi/content/full/299/5612/1557/DC1

Movies S1 and S2

20 November 2002; accepted 27 January 2003